

Eigenvalue Analysis of Thin Plate with Complicated Shapes By a Novel Infinite Element Method

Deshin Liu¹ and Yuwei Chen^{1,*}

Abstract: A novel infinite element method (IEM) is presented for solving plate vibration problems in this paper. In the proposed IEM, the substructure domain is partitioned into multiple layers of geometrically similar finite elements which use only the data of the boundary nodes. A convergence criterion based on the trace of the mass matrix is used to determine the number of layers in the IE model partitioning process. Furthermore, in implementing the Craig-Bampton (CB) reduction method, the inversion of the global stiffness matrix is calculated using only the stiffness matrix of the first element layer. The validity and performance of the proposed method are investigated by means of four illustrative problems. The first example considers the case of a simple clamped rectangular plate. It is observed that the IEM results are consistent with the theoretical results for first six natural frequencies. The second example considers the frequency response of a clamped rectangular plate with a crack. The main feature of IEM is that a very fine and good quality virtual mesh can be created around the crack tip. The third and fourth examples consider the natural frequency of a multiple point supported plate and a perforated plate, respectively. The results are obtained just need to adjust the reference point or boundary nodes. The parametric analyses for various geometric profiles are easy to be conducted using these numerical techniques. In general, the results presented in this study have shown that the proposed method provides a direct, convenient and accurate tool for eigenvalue analysis of thin plate structure with complicated shapes.

Keywords: Infinite element method, Craig-Bampton method, plate vibration, eigenvalue problem.

1 Introduction

The classical finite element method solving large structural or singularity problems usually requires the construction of a large number of elements, resulting in insufficient computer memory or slow computation. Therefore, many scholars have proposed methods to reduce the degree of freedom of the model (such as Irons-Guyan reduction method, modal synthesis method, etc.) or other numerical methods (such as boundary element method, meshless method, etc.) to solve the above problems. The similarity of elements is also one of the numerical methods.

Thatcher [Thatcher (1975)] combines the concepts of finite element methods and similarity

¹ Department of Mechanical Engineering and Advanced Institute of Manufacturing with High-Tech Innovations, National Chung-Cheng University, Minhsiung, Chiayi 62102, Taiwan.

* Corresponding Author: Yuwei Chen. Email: ywc0314@gmail.com.

to create many refined triangle elements near a singularity to approximate the solution. For the problem of cracked structural, Ying [Ying (1978)] produces a number of similar triangular elements near the crack tip and combines them into a single element, was called infinite similar element method (ISEM). Han et al. [Han and Ying (1979); Han and Ying (1982)] continue to study the derivation and application of the ISEM, the many elements are reduced into a super-element using elemental similarity, and consider the inertial effect, was called infinite element method (IEM). Ying [Ying (1992)] proved that there exists a transformation matrix to relate the nodal displacement vector between the inner and outer layers, therefore the total stiffness matrix could reduce to form a combined stiffness matrix related only to boundary nodes. Notably, it was shown that the combined stiffness matrix could converge to a certain constant quantity as the number of layers approached to infinity. Liu has been working on the study of the IEM since the 2000s. Liu et al. [Liu and Chiou (2003a); Liu and Chiou (2003b)] proposed a hybrid IE-FE model to analyze elastic problems with multiple cracks. Liu et al. [Liu, Zhuang and Chung (2009)] extended the IE-FE formalism to model and analyze moisture diffusion in a heterogeneous epoxy resin containing multiple randomly distributed particles. In a later study, Liu et al. [Liu, Tu and Chung (2013)] proposed a Plate IEM (PIEM) algorithm based on Mindlin-Reissner theory to investigate the bending strength of plates with through-thickness holes. According to the above literature, most scholars use the similarity of elements to degrade IEM to the boundary nodes. Although the amount of computing can be greatly reduced in these methods, the accuracy of the higher natural frequency is somewhat inadequate.

In earlier works, Guyan [Guyan (1965)], Irons [Irons (1965)] and Kidder [Kidder (1973)] proposed the reduction procedures to degenerate the mass/stiffness matrix of the FE domain, respectively. However, the accuracy decreased because of the neglect of the inertial effect in the reduction procedures for dynamic analysis. Component mode synthesis (CMS) is a dynamic matrix reduction method. Hurty [Hurty (1965)] first proposed a component mode synthesis that used rigid-body modes, redundant-interface modes and fixed-interface normal modes to form a structural modal matrix. Craig and Bampton [Craig and Bampton (1968)] simplified Hurty's method, proposed the constraint modes and fixed-interface normal modes to form a structural modal matrix, this scheme is called Craig-Bampton method (CBM). Saito et al. [Saito, Castanier and Pierre (2006)], Gupta et al. [Gupta, Hussein, Degrande et al. (2007)] and Kim et al. [Kim, Kim and Yoo (2010)] used CBM reduction techniques to simplify complex models, respectively. Liu and Lin [Liu and Lin (2016)] integrated Craig-Bampton method with a dynamic infinite element (DIE) formulation to analyze the membrane vibration problem. Liu et al. [Liu and Chen (2018)] improved the efficiency of the CBM reduction for DIE model. The efficiency of the CBM reduction process is improved by using a numerically recursive procedure to calculate the inversion of stiffness matrix.

Based on the Liu et al. [Liu and Chen (2018)] proposed scheme, eigenvalue analysis of thin plate with complicated shapes are investigated in this paper. First, an infinite element model of the Mindlin-Reissner plate is created, and then the model is reduced adopting the Craig-Bampton method. In Mindlin-Reissner plate theory, the conventional IEM algorithm cannot be applied. The stiffness matrix needs to be disassembled and recombined to obtain the similarity between the element layers. The validity and performance of the proposed method are studied by means of four familiar thin plate structures with complicated shape, involve a

rectangular plate, a side cracked plate, a multiple point supported plate, and a perforated plate.

2 Infinite element method

2.1 Finite element formulation of mindlin-reissner plate

Mindlin-Reissner plate theory [Mindlin (1951)] is an extension of Kirchhoff-Love plate theory [Love (1888)] which takes into account shear deformations through the thickness of the plate. The equation of motion of the plate is established as:

$$[M]\{\ddot{\delta}\} + [K]\{\delta\} = 0 \quad (1)$$

with mass matrix $[M]$, stiffness matrix $[K]$ and the displacement vector $\{\delta\}$. From Mindlin-Reissner plate theory, the displacement $\{\delta\} = \{u, v, w\}^T$ have the form given in Eq. (2).

$$\begin{cases} u = -z\theta_x(x, y) = -z\left(\frac{\partial w}{\partial x} - \gamma_{xz}\right) \\ v = -z\theta_y(x, y) = -z\left(\frac{\partial w}{\partial y} - \gamma_{yz}\right) \\ w = w(x, y) \end{cases} \quad (2)$$

where x and y are in-plane axes located at the mid-plane of the plate, and z is along the direction of plate thickness as seen in Fig. 1.

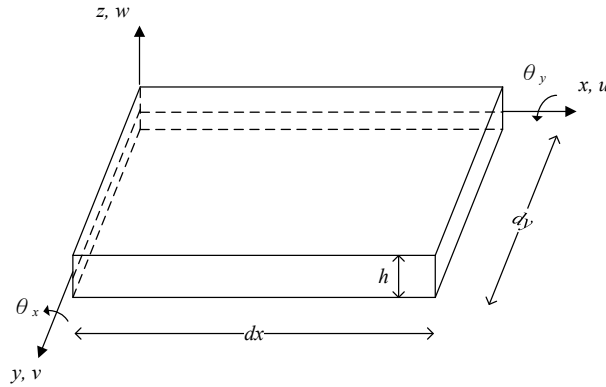


Figure 1: Coordinate frame of the plate element.

The θ_x and θ_y are the rotations of the mid-plane about the y and x axes, respectively; and γ is the angle caused by the transverse shear deformation. Mapping from the physical coordinates to the natural coordinates, the rotate and transverse displacements can be expressed as:

$$\begin{cases} \theta_x = \sum_{i=1}^n H_i(\zeta, \eta)(\theta_x)_i \\ \theta_y = \sum_{i=1}^n H_i(\zeta, \eta)(\theta_y)_i \\ w = \sum_{i=1}^n H_i(\zeta, \eta)w_i \end{cases} \quad (3)$$

where H_i are the 4-node plate finite element shape functions, and (ζ, η) is represented as natural coordinates. From that the element matrices are established as:

$$\begin{cases} [K^e] = [K_b^e] + [K_s^e] \\ \quad = \frac{h^3}{12} \int_{-1}^1 \int_{-1}^1 [B_b]^T [D_b] [B_b] \det[J] d\zeta d\eta + \kappa h \int_{-1}^1 \int_{-1}^1 [B_s]^T [D_s] [B_s] \det[J] d\zeta d\eta \\ [M^e] = \rho \int_{-1}^1 \int_{-1}^1 [N]^T [I] [N] \det[J] d\zeta d\eta \end{cases} \quad (4)$$

where the $[K_b^e]$ is the bending stiffness matrix and $[K_s^e]$ is the shear stiffness matrix, in which h is the thickness of the plate, κ is the shear energy correction factor, and $[J]$ is the Jacobian matrix:

$$[J] = \begin{bmatrix} \frac{\partial x}{\partial \zeta} & \frac{\partial y}{\partial \zeta} \\ \frac{\partial x}{\partial \eta} & \frac{\partial y}{\partial \eta} \end{bmatrix} \quad (5)$$

$[B_b]$, $[B_s]$ and $[N]$ consist of the shape functions as listed in Eqs. (6)-(8), respectively. In addition, $[D_b]$, $[D_s]$ and $[I]$ are related to dimension or material properties of model as listed in Eqs. (9)-(11), respectively.

$$[B_b] = \begin{bmatrix} \frac{\partial H_1}{\partial x} & 0 & 0 & \frac{\partial H_2}{\partial x} & 0 & 0 & \dots & \frac{\partial H_4}{\partial x} & 0 & 0 \\ 0 & \frac{\partial H_1}{\partial y} & 0 & 0 & \frac{\partial H_2}{\partial y} & 0 & \dots & 0 & \frac{\partial H_4}{\partial y} & 0 \\ \frac{\partial H_1}{\partial y} & \frac{\partial H_1}{\partial x} & 0 & \frac{\partial H_2}{\partial y} & \frac{\partial H_2}{\partial x} & 0 & \dots & \frac{\partial H_4}{\partial y} & \frac{\partial H_4}{\partial x} & 0 \end{bmatrix} \quad (6)$$

$$[B_s] = \begin{bmatrix} -H_1 & 0 & \frac{\partial H_1}{\partial x} & -H_2 & 0 & \frac{\partial H_2}{\partial x} & \dots & -H_4 & 0 & \frac{\partial H_4}{\partial x} \\ 0 & -H_1 & \frac{\partial H_1}{\partial y} & 0 & -H_2 & \frac{\partial H_2}{\partial y} & \dots & 0 & -H_4 & \frac{\partial H_4}{\partial y} \end{bmatrix} \quad (7)$$

$$[N] = \begin{bmatrix} H_1 & 0 & 0 & H_2 & 0 & 0 & \cdots & H_4 & 0 & 0 \\ 0 & H_1 & 0 & 0 & H_2 & 0 & \cdots & 0 & H_4 & 0 \\ 0 & 0 & H_1 & 0 & 0 & H_2 & \cdots & 0 & 0 & H_4 \end{bmatrix} \quad (8)$$

$$[D_b] = \frac{E}{1-\nu^2} \begin{bmatrix} 1 & \nu & 0 \\ \nu & 1 & 0 \\ 0 & 0 & \frac{1-\nu}{2} \end{bmatrix} \quad (9)$$

$$[D_s] = \frac{E}{2(1-\nu)} \begin{bmatrix} 1 & 0 \\ 0 & 1 \end{bmatrix} \quad (10)$$

$$[I] = \begin{bmatrix} \frac{h^3}{12} & 0 & 0 \\ 0 & \frac{h^3}{12} & 0 \\ 0 & 0 & h \end{bmatrix} \quad (11)$$

2.2 Infinite element model

The basic concept of IE model as shown in Fig. 2, the computational domain is partitioned into multiple layers of geometrically-similar elements. For element *I*, the local nodes *i* are numbered 1, 2, 3, and 4 in the counterclockwise direction, and (x_i^I, y_i^I) denotes the global coordinate value of node *i*. By taking the global origin *O* and *c* as the center of the similarity and the proportionality ratio, respectively, the element *II* is created. The global coordinates of elements *I* and *II* are related as shown in Eq. (12). From Eq. (12), and recalling Eq. (5), the determinants of the Jacobian matrices of the element *I* and *II* are related as shown in Eq. (13). Similarly, from Eq. (12), and recalling Eq. (6), the relation of $[B_b]$ of the element *I* and *II* can be shown in Eq. (14) [Liu and Chiou (2003a)].

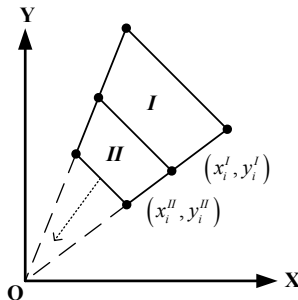


Figure 2: Schematic representation of geometrically-similar 2D elements in IE formulation

$$(x_i'', y_i'') = (cx_i', cy_i') \quad (12)$$

$$\det[J]'' = c^2 \det[J]' \quad (13)$$

$$[B_b]'' = \frac{1}{c} [B_b]' \quad (14)$$

Therefore, as shown in Eq. (15), the mass matrix $[M]$ and bending stiffness matrix $[K_b]$ of the first and second element layers are related. The matrices of the first element layer have the forms shown in Eq. (16), where the mass matrix is transformed as a diagonal matrix by a lumped-mass formulation.

$$\begin{cases} [M]'' = c^2 [M]' \\ [K_b]'' = [K_b]' \end{cases} \quad (15)$$

$$\begin{cases} [M]' = \begin{bmatrix} M_1 & -D \\ -D^T & M_2 \end{bmatrix} = \begin{bmatrix} L_1 & 0 \\ 0 & L_2 \end{bmatrix} \\ [K_b]' = \begin{bmatrix} K_1 & -A \\ -A^T & K_2 \end{bmatrix} \end{cases} \quad (16)$$

From Eq. (15), the four-node elements I and II can both be mapped using the same square-shaped master element. In other words, these elements are designated as similar elements when the coordinate of an element is similar to other elements. Combining the matrices from first to n -th element layer, the mass and bending stiffness matrices can be established as in Eq. (17) and Eq. (18).

$$[M]_{IE} = \begin{bmatrix} L_1 & 0 & 0 & 0 & 0 & 0 \\ 0 & R & 0 & 0 & 0 & 0 \\ 0 & 0 & c^2 R & 0 & 0 & 0 \\ 0 & 0 & 0 & \ddots & 0 & 0 \\ 0 & 0 & 0 & 0 & c^{2(n-2)} R & 0 \\ 0 & 0 & 0 & 0 & 0 & c^{2(n-1)} L_2 \end{bmatrix} \quad (17)$$

$$[K_b]_{IE} = \begin{bmatrix} K_1^b & -A & 0 & 0 & 0 & 0 \\ -A^T & Q & -A & 0 & 0 & 0 \\ 0 & -A^T & Q & -A & 0 & 0 \\ 0 & 0 & \ddots & \ddots & \ddots & 0 \\ 0 & 0 & 0 & -A^T & Q & -A \\ 0 & 0 & 0 & 0 & -A^T & K_2^b \end{bmatrix} \quad (18)$$

where $R = L_1 + c^2 L_2$ and $Q = K_1 + K_2$. For shear stiffness, let the matrix $[B_s]$ be partitioned into two submatrices:

$$\begin{aligned}
[B_s] &= [B_s^*] + [B_s^{**}] \\
&= \begin{bmatrix} 0 & 0 & \frac{\partial H_1}{\partial x} & 0 & 0 & \frac{\partial H_2}{\partial x} & \dots \\ 0 & 0 & \frac{\partial H_1}{\partial y} & 0 & 0 & \frac{\partial H_2}{\partial y} & \dots \end{bmatrix} + \begin{bmatrix} -H_1 & 0 & 0 & -H_2 & 0 & 0 & \dots \\ 0 & -H_1 & 0 & 0 & -H_2 & 0 & \dots \end{bmatrix} \quad (19)
\end{aligned}$$

Substituting Eq. (19) into Eq. (4), the shear stiffness is re-represented as follow:

$$[K_s] = [K_s^*] + [K_s^{**}] + [K_s^{***}] \quad (20)$$

where

$$\begin{cases} [K_s^*] = \kappa h \int_{-1}^1 \int_{-1}^1 [B_s^*]^T [D_s] [B_s^*] \det[J] d\zeta d\eta \\ [K_s^{**}] = \kappa h \int_{-1}^1 \int_{-1}^1 \left([B_s^*]^T [D_s] [B_s^{**}] + [B_s^{**}]^T [D_s] [B_s^*] \right) \det[J] d\zeta d\eta \\ [K_s^{***}] = \kappa h \int_{-1}^1 \int_{-1}^1 [B_s^{**}]^T [D_s] [B_s^{**}] \det[J] d\zeta d\eta \end{cases} \quad (21)$$

According to geometric similarity, the relationship of the shear stiffness matrix between the first and second element layers is:

$$[K_s]^H = [K_s^*]^I + c [K_s^{**}]^I + c^2 [K_s^{***}]^I \quad (22)$$

where the submatrices of the first element layer are shown as:

$$\begin{cases} [K_s^*]^I = \begin{bmatrix} K_1^* & -A_1^{*T} \\ -A_1^* & K_2^* \end{bmatrix} \\ [K_s^{**}]^I = \begin{bmatrix} K_1^{**} & -A_1^{**T} \\ -A_1^{**} & K_2^{**} \end{bmatrix} \\ [K_s^{***}]^I = \begin{bmatrix} K_1^{***} & -A_1^{***T} \\ -A_1^{***} & K_2^{***} \end{bmatrix} \end{cases} \quad (23)$$

Similarly, combining the shear stiffness matrices from first to n -th element layer, can be established as:

$$[K_s]_{IE} = \begin{bmatrix} K_1^s & -A_1 & 0 & 0 & 0 & 0 \\ -A_1^T & Q_2 & -A_2 & 0 & 0 & 0 \\ 0 & -A_2^T & Q_3 & -A_3 & 0 & 0 \\ 0 & 0 & \ddots & \ddots & \ddots & 0 \\ 0 & 0 & 0 & -A_{n-1}^T & Q_n & -A_n \\ 0 & 0 & 0 & 0 & -A_n^T & K_2^s \end{bmatrix} \quad (24)$$

where

$$\begin{cases} K_1^s = K_1^* + K_1^{**} + K_1^{***} \\ K_2^s = K_2^* + c^{(n-1)}K_2^{**} + c^{2(n-1)}K_2^{***} \\ A_i = A^* + c^{(i-1)}A^{**} + c^{2(i-1)}A^{***}, \quad i = 1, 2, \dots, n \\ Q_i = Q^* + c^{(i-2)}Q^{**} + c^{2(i-2)}Q^{***}, \quad i = 2, 3, \dots, n \end{cases} \quad (25)$$

Recalling Eq. (1), the eigenvalue formulation can be obtained by assembling the aforementioned equations follows:

$$\left([K]_{IE} - \omega^2 [M]_{IE} \right) \{u\}_{IE} = 0 \quad (26)$$

where

$$[K]_{IE} = [K_b]_{IE} + [K_s]_{IE} \quad (27)$$

$$\{u\}_{IE} = \{ \delta_0 \quad \delta_1 \quad \delta_2 \quad \dots \quad \delta_{n-1} \quad \delta_n \}^T \quad (28)$$

The convergence analysis of element number is necessary before the numerical analysis. In practice, the convergence of the mass matrix depends on the number of element layers in the IE model. For dynamic problems, the trace of the mass matrix will converge to a constant [Liu and Chen (2018)]:

$$Tr[M]_{IE}^{(n)} = Tr \left(L_1 + c^{2(n-1)}L_2 + \sum_{N=2}^n c^{2(N-2)}R \right) \quad (29)$$

if $c < 1$, then

$$\lim_{n \rightarrow \infty} Tr[M]_{IE}^{(n)} = Tr[M]_{IE} \quad (30)$$

where n denotes the number of chosen element layers, and $Tr[M]_{IE}$ converges to a constant as the number of element layers approaches infinity.

2.3 Model reduction

In this study, the Craig-Bampton reduction procedure [Craig and Bampton (1968)] is adopted to reduce the infinite element model. The mass and stiffness matrices and displacement vector in the Eq. (26) can be partitioned respectively as:

$$[M]_{IE} = \begin{bmatrix} M^{BB} & 0 \\ 0 & M^{II} \end{bmatrix} = \begin{bmatrix} L_1 & 0 & 0 & 0 & 0 & 0 \\ 0 & R & 0 & 0 & 0 & 0 \\ 0 & 0 & c^2R & 0 & 0 & 0 \\ 0 & 0 & 0 & \ddots & 0 & 0 \\ 0 & 0 & 0 & 0 & c^{2(n-2)}R & 0 \\ 0 & 0 & 0 & 0 & 0 & c^{2(n-1)}L_2 \end{bmatrix} \quad (31)$$

$$[K]_{IE} = \begin{bmatrix} K^{BB} & K^{BI} \\ K^{IB} & K^{II} \end{bmatrix} = \left[\begin{array}{c|cccccc} K'_1 & -A'_1 & 0 & 0 & 0 & 0 \\ \hline -A_1^{T'} & Q'_2 & -A'_2 & 0 & 0 & 0 \\ 0 & -A_2^{T'} & Q'_3 & -A'_3 & 0 & 0 \\ 0 & 0 & \ddots & \ddots & \ddots & 0 \\ 0 & 0 & 0 & -A_{n-1}^{T'} & Q'_n & -A'_n \\ 0 & 0 & 0 & 0 & -A_n^{T'} & K'_2 \end{array} \right] \quad (32)$$

$$= \left[\begin{array}{c|cccccc} K_1^b & -A & 0 & 0 & 0 & 0 \\ \hline -A^T & Q & -A & 0 & 0 & 0 \\ 0 & -A^T & Q & -A & 0 & 0 \\ 0 & 0 & \ddots & \ddots & \ddots & 0 \\ 0 & 0 & 0 & -A^T & Q & -A \\ 0 & 0 & 0 & 0 & -A^T & K_2^b \end{array} \right] + \left[\begin{array}{c|cccccc} K_1^s & -A_1 & 0 & 0 & 0 & 0 \\ \hline -A_1^T & Q_2 & -A_2 & 0 & 0 & 0 \\ 0 & -A_2^T & Q_3 & -A_3 & 0 & 0 \\ 0 & 0 & \ddots & \ddots & \ddots & 0 \\ 0 & 0 & 0 & -A_{n-1}^T & Q_n & -A_n \\ 0 & 0 & 0 & 0 & -A_n^T & K_2^s \end{array} \right] \quad (33)$$

$$\{u\}_{IE} = \begin{Bmatrix} u^B \\ u^I \end{Bmatrix} = \{\delta_0 \ \dots \ \delta_1 \ \delta_2 \ \dots \ \delta_{s-1} \ \delta_s\}^T$$

where the vectors u^B and u^I denote physical displacements of boundary and interior points, respectively. In the Craig-Bampton reduction procedure, the coordinate transformation relating the modal coordinate to the physical coordinates is:

$$\{u\}_{IE} = \begin{Bmatrix} u^B \\ u^I \end{Bmatrix} = \begin{bmatrix} I & 0 \\ \phi^C & \phi^N \end{bmatrix} \begin{Bmatrix} p^B \\ p^N \end{Bmatrix} = [\phi] \{p\}, \quad p^B \equiv u^B \quad (34)$$

where the constraint modes $[\phi^C]$ are defined as the mode shapes of the interior freedoms due to successive unit displacements of the boundary points, with all other boundary points being totally constrained:

$$\{u^I\} = -[K^{II}]^{-1} [K^{IB}] \{u^B\} \equiv [\phi^C] \{u^B\} \quad (35)$$

And the normal modes $[\phi^N]$ are defined as the normal modes with totally constrained boundary. Thus, they are the eigenvectors of the eigenvalue problem:

$$\{u^I\} = \{\phi^I\} e^{i\omega t}, \quad \left([I] - \omega^2 [K^{II}]^{-1} [M^{II}] \right) \{\phi^I\} = 0 \quad (36)$$

$$[\phi^N] = [\phi_1^I \ \phi_2^I \ \phi_3^I \ \dots] \quad (37)$$

Recalling Eq. (32), $[K^{II}]$ is a symmetric block-tridiagonal matrix. Therefore, the inversion of $[K^{II}]$ can be expressed as a semi-separable matrix:

$$[K^H]^{-1} = \begin{bmatrix} U_1 V_1^T & U_1 V_2^T & U_1 V_3^T & \cdots & U_1 V_n^T \\ V_2 U_1^T & U_2 V_2^T & U_2 V_3^T & \cdots & U_2 V_n^T \\ V_3 U_1^T & V_3 U_2^T & U_3 V_3^T & \cdots & U_3 V_n^T \\ \vdots & \vdots & \vdots & \ddots & \vdots \\ V_n U_1^T & V_n U_2^T & V_n U_3^T & \cdots & U_n V_n^T \end{bmatrix} \quad (38)$$

where matrices $[U_i]$ and $[V_i]$ are computed as follow:

$$\begin{cases} U_1 = I \\ U_2 = A_2'^{-1} Q_2' \\ U_{i+1} = A_{i+1}'^{-1} (Q_{i+1}' U_i - A_i^{T'} U_{i-1}), \quad i = 2, \dots, n-1 \\ V_n^T = (K_2' U_n - A_n^{T'} U_{n-1})^{-1} \\ V_{n-1}^T = V_n^T K_2' A_n^{-1'} \\ V_i^T = (V_{i+1}^T Q_{i+2}' - V_{i+2}^T A_{i+2}^{T'}) A_{i+1}^{-1'}, \quad i = n-2, \dots, 1 \end{cases} \quad (39)$$

Denoting the diagonal blocks of $[K^H]^{-1}$ as D_i , that can be obtained recursively as follow [Jain, Li, Cauley et al. (2007)]:

$$\begin{cases} D_1 = (Q_2' - A_2' S_1^T)^{-1} \\ D_i = (Q_{i+1}' - A_{i+1}' S_i^T)^{-1} (I + A_i^{T'} D_{i-1} S_{i-1}), \quad i = 2, \dots, n-1 \\ D_n = K_2'^{-1} (I + A_n^{T'} D_{n-1} S_{n-1}) \end{cases} \quad (40)$$

where matrices $[S_i]$ are defined as follow:

$$V_{i+1}^T = V_i^T S_i \quad (41)$$

And $[S_i]$ are computed using the following numerically recursive procedure:

$$\begin{cases} S_{n-1} = A_n' K_2'^{-1} \\ S_i = A_{i+1}' (Q_{i+2}' - S_{i+1} A_{i+2}^{T'})^{-1}, \quad i = n-2, \dots, 1 \end{cases} \quad (42)$$

The inversion of $[K^H]$ can be rewritten as follow:

$$[K^{II}]^{-1} = \begin{bmatrix} D_1 & D_1 S_1 & D_1 S_1 S_2 & \cdots & D_1 S_1 \cdots S_{n-1} \\ (D_1 S_1)^T & D_2 & D_2 S_2 & \cdots & D_2 S_2 \cdots S_{n-1} \\ (D_1 S_1 S_2)^T & (D_2 S_2)^T & D_3 & \cdots & D_3 S_3 \cdots S_{n-1} \\ \vdots & \vdots & \vdots & \ddots & \vdots \\ (D_1 S_1 \cdots S_{n-1})^T & (D_2 S_2 \cdots S_{n-1})^T & (D_3 S_3 \cdots S_{n-1})^T & \cdots & D_n \end{bmatrix} \quad (43)$$

where the $[K^{II}]^{-1}$ is calculated using only the stiffness matrix of the first element layer. Substituting Eq. (34) into Eq. (26), the eigenequation can be obtained by substituting the coordinate transformation relation:

$$([\phi]^T [K]_{IE} [\phi] - \omega^2 [\phi]^T [M]_{IE} [\phi]) \{p\} = 0 \quad (44)$$

3 Case studies

3.1 Rectangular plate

Consider a rectangular plate shown in Fig. 3(a). Let the plate geometric conditions and material properties be given as follows: $a=1.2$ m, $b=1.0$ m, thickness $h=0.01$ m, mass density $\rho=7800$ kg/m³, Young’s modulus $E=200$ GPa, and Poisson’s ratio $\nu=0.3$. Furthermore, assume that the plate is clamped on all four sides, the natural frequency $\omega_{m,n}$ are estimated respectively as:

$$\omega_{m,n} = \left[\left(\frac{m}{a} \right)^2 + \left(\frac{n}{b} \right)^2 \right] \sqrt{\frac{D\pi^4}{2\rho h}}, \quad m, n = 1, 2, \dots \quad (45)$$

In implementing the IE model, 88 nodes are deployed at the boundary, and the virtual mesh pattern is shown in Fig. 3(b). For an ideal element, the aspect ratio should have a value of 1.0, so the ratio should be equal to 0.875 in this case. A number of required c element layer $s=40$ is obtained by the convergence criterion Eq. (30). The convergence process is shown in Fig. 4. Based on the above results, for more accurate results, the number of layers, s , is 40 and the proportionality ratio, c , is 0.875 with respect to the related similar partition centers. The first six mode shapes of the rectangular plate are depicted in Fig. 5. The results for the six lowest natural frequencies are shown in Tab. 1 with the theoretical results, where the relative difference is less than 0.5%. Comparing the sets of natural frequencies reveals, the IEM results are in satisfactory agreement with the theoretical results.

Table 1: First six natural frequencies of clamped rectangular plate (Hz)

Methods	Mode No.					
	1	2	3	4	5	6
Exact solution	40.78	90.93	113.00	163.14	174.51	233.35
IEM	40.65	90.73	112.90	162.91	174.94	233.99
R.D. (%)	0.32	0.22	0.09	0.14	0.25	0.27

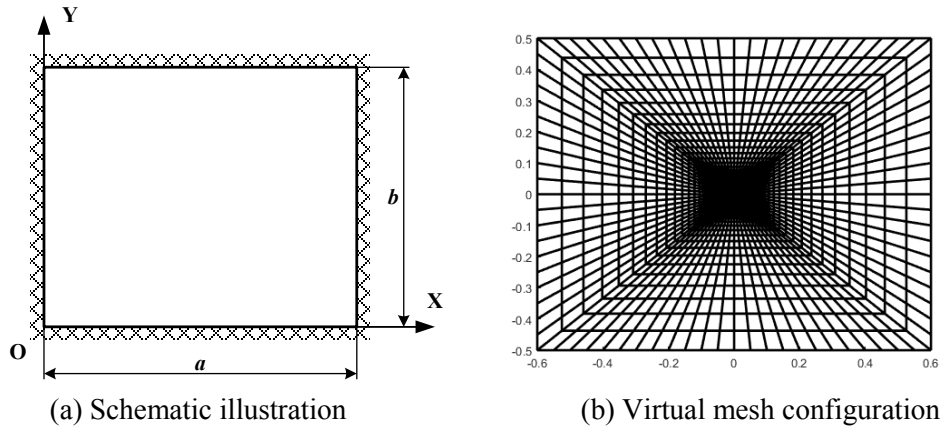


Figure 3: Schematic illustration and virtual mesh configuration of the clamped rectangular plate

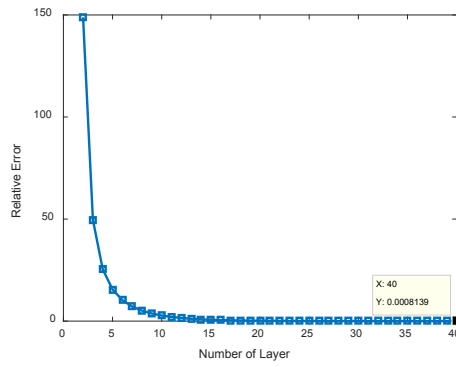


Figure 4: The convergence process of the required virtual element layer

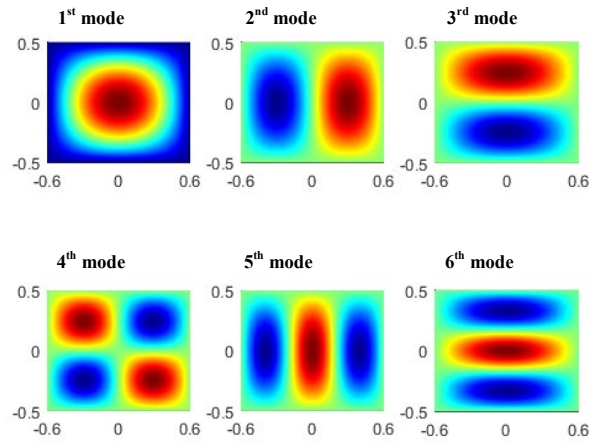
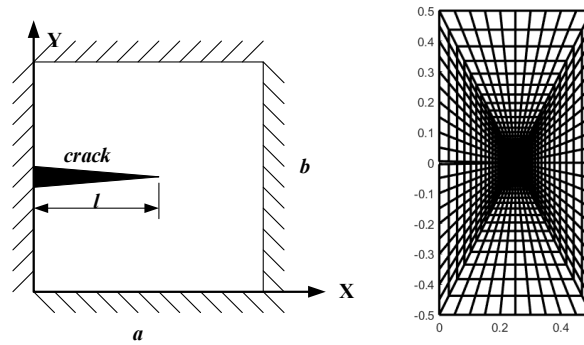


Figure 5: First six mode shapes of clamped rectangular plate

3.2 Cracked plate

Considering a rectangular plate with a side through-thickness crack, and the crack has a length l , is shown in Fig. 6(a). The plate is assumed be clamped on all the sides. The geometric conditions of the plate are assigned as follows: $a=0.5$ m, $b=1.0$ m, thickness $h=0.01$ m. The same material properties are assigned as previous example: mass density $\rho=7800$ kg/m³, Young's modulus $E=200$ GPa, and Poisson's ratio $\nu=0.3$. In this study, the crack length is assigned various values in the range of $l=0.1\sim 0.4$ m. The proportionality ratio is set as $c=0.875$, and number of virtual element layer $s=40$ as in the previous example. Fig. 6(b) shows the virtual mesh configuration and virtual node arrangement of the IE model. Given various crack lengths, the results obtained from the proposed IEM for the six lowest natural frequencies as shown in Fig. 7. The results show that the fourth and fifth frequencies are highly sensitive to the crack length. Fig. 8 shows the first six mode shapes given crack lengths of $l=0.1, 0.2, 0.3,$ and 0.4 m, respectively.

Using these efficient numerical techniques, a very fine and good quality grid pattern can be created around each crack tip without many freedoms. Furthermore, the results of obtaining IEM only need to adjust the reference point, that is easily allowed to conduct parametric analysis for various crack lengths.



(a) Schematic illustration (b) Virtual mesh configuration

Figure 6: Schematic illustration and virtual mesh configuration of the cracked plate

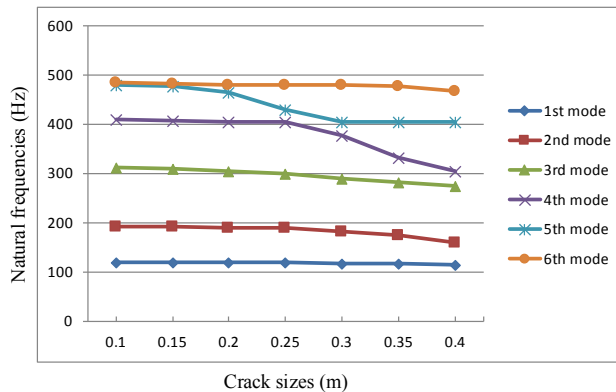


Figure 7: First six natural frequencies of cracked plate (Hz)

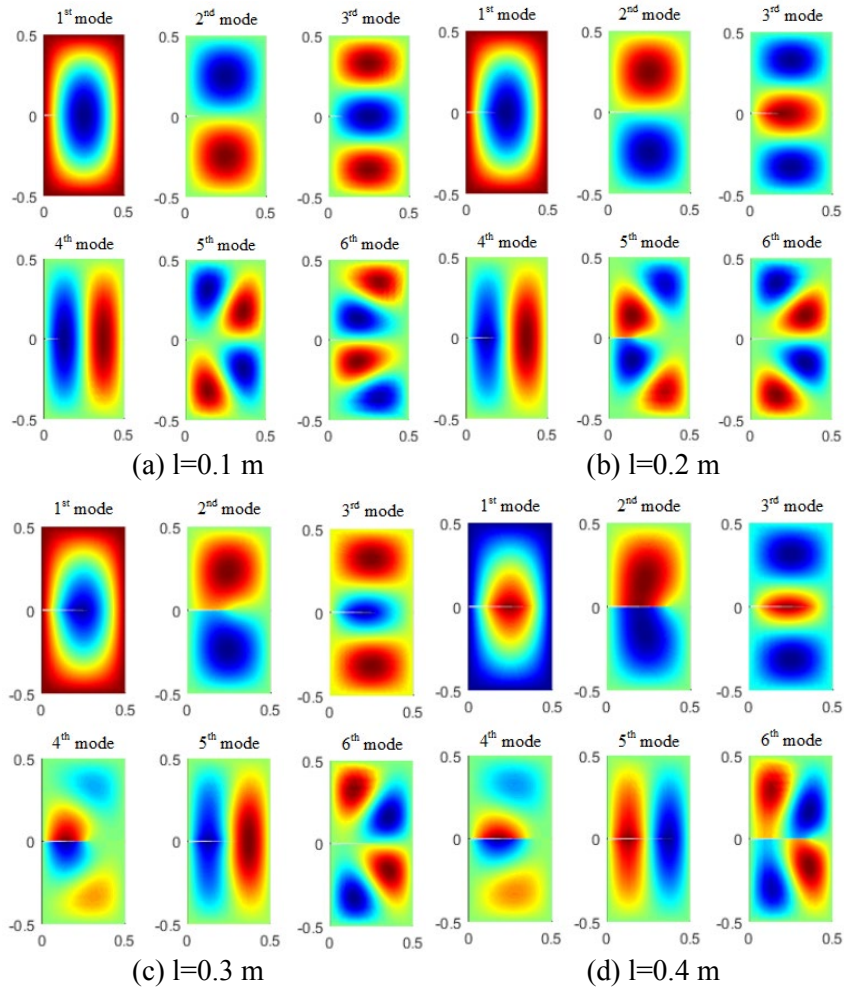
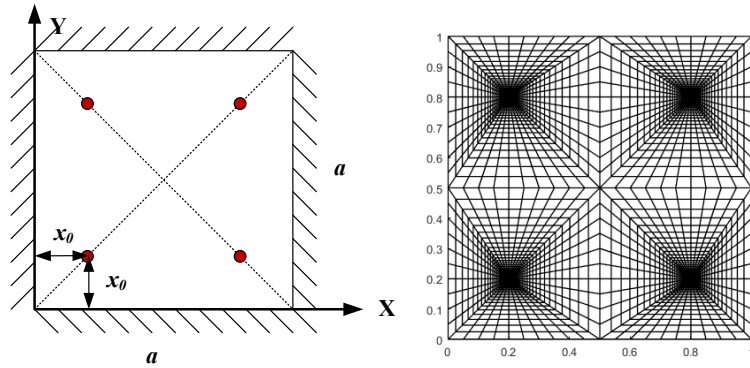


Figure 8: First six mode shapes of cracked plate

3.3 Multiple point supported plate

Considering a multiple point supported plate is shown in Fig. 9(a), a square plate is locked on the four symmetrically point supports. The dimensions of the plate are assigned as follows: $a=1$ m and thickness $h=0.01$ m, and the same material properties as first example. Fig. 9(b) shows the virtual mesh configuration and virtual node arrangement of the corresponding model. The model consists of four subdomains, each of which is an IE model. As shown, the reference points are set at the support points, respectively. The proportionality ratio c and number of virtual element layer s are same as the first example. Fig. 10 shows the six lowest natural frequencies obtained from IEM, and consider the support position is shifted from $x_0=0.1$ m to $x_0=0.4$ m. The maximum fundamental frequency is achieved in the range around $x_0=0.175\sim 0.275$ m. Li et al. [Li, Tian, Wang et al. (2016)] have confirmed this finding. Fig. 11 shows the first six mode shapes given support positions of $x_0=0.1, 0.2, 0.3,$ and 0.4 m, respectively. The results show that the

rectangular plate begins to weaken significantly when the support position x_0 is shifted over 0.25 m. In addition, the sixth natural frequency is decreased but not apparent when the support position x_0 is shifted over 0.25 m. That mainly due to the supports are closed enough to the center of the thin plate, so that has little effect for the natural frequencies and mode shapes of sixth mode. As in the second example, the results of obtaining IEM only need to adjust the reference point. It is easily allowed to conduct parametric analysis for various support position. Furthermore, this example demonstrates the feasibility of combining IEM subdomains.



(a) Schematic illustration (b) Virtual mesh configuration

Figure 9: Schematic illustration and virtual mesh configuration of the multiple supported plate

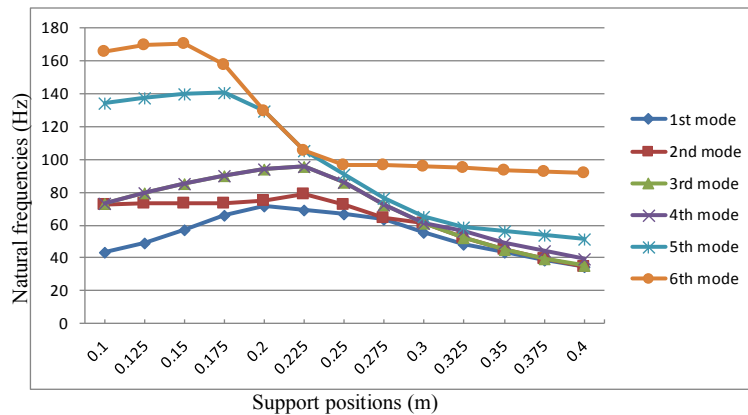


Figure 10: First six natural frequencies of the multiple point supported plate (Hz)

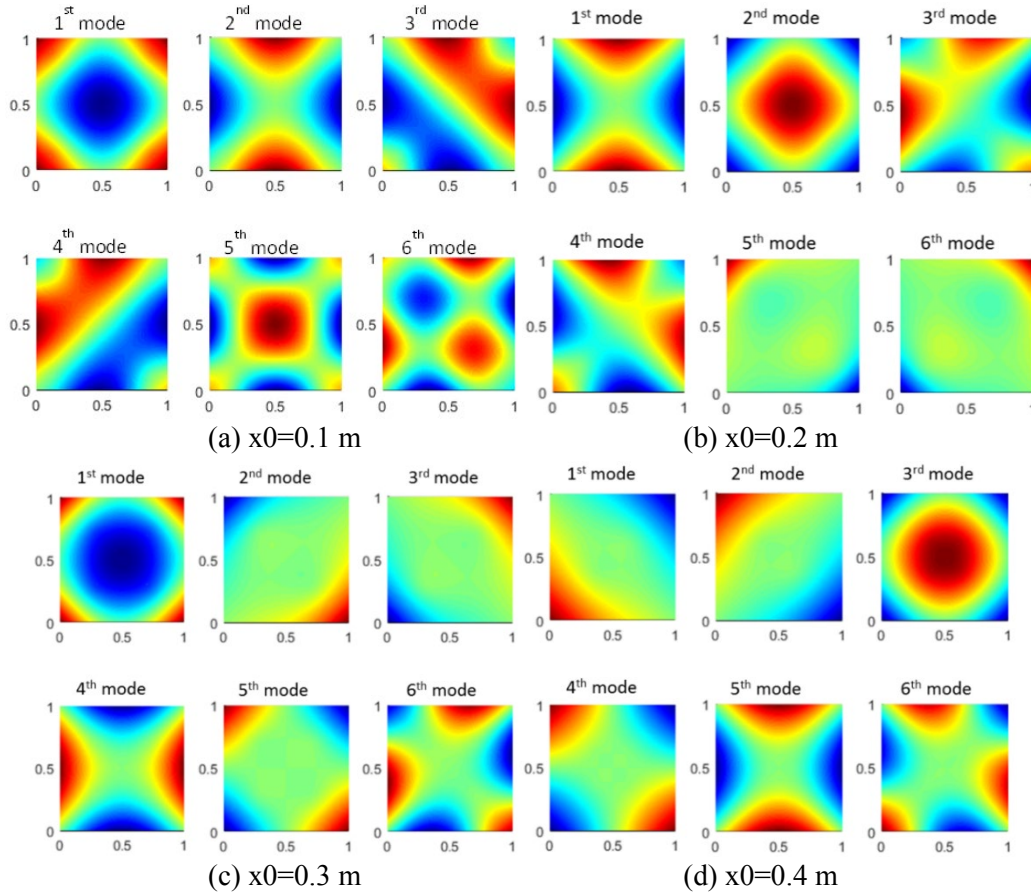


Figure 11: First six mode shapes of the multiple point supported plate

3.4 Perforated plate

Considering a perforated plate is shown in Fig. 12(a), where the dimensions of the plate are assigned as follows: $a=0.8$ m and thickness $h=0.01$ m, and the same material properties as first example. The plate is assumed be clamped on all four sides and the circle holes have a radius r . The circle hole radius r is assigned various values in the range of $r=0.03\sim 0.07$ m in this study. Fig. 12(b) shows the virtual mesh configuration and virtual node arrangement of the corresponding model. The model consists of sixteen subdomains, each of which is the same IE model. The proportionality ratio c and number of virtual element layer s are same as the first example. Fig. 13 shows the six lowest natural frequencies given various circle hole sizes. Fig. 14 shows the first six mode shapes given hole radius of $r=0.03, 0.04, 0.05, 0.06$, and 0.07 m, respectively.

This is another case to show the advantage of IEM. The results are obtained just need to adjust the boundary nodes of one subdomain. The parametric analyses for various circle hole radius are easy to be conducted. Furthermore, this example not only demonstrates the feasibility of combining IEM subdomains, but also copying.

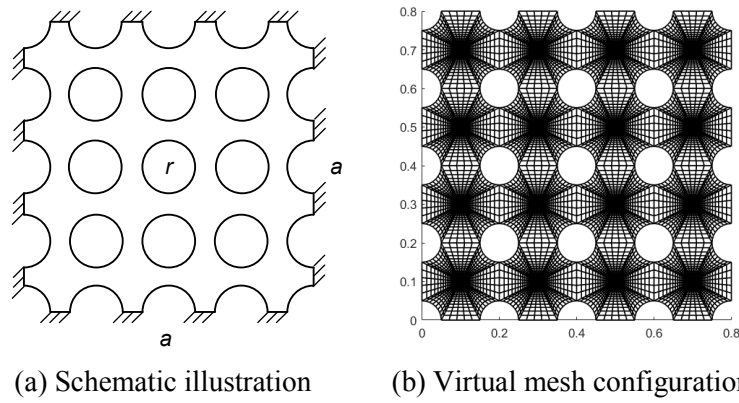


Figure 12: Schematic illustration and virtual mesh configuration of the perforated plate

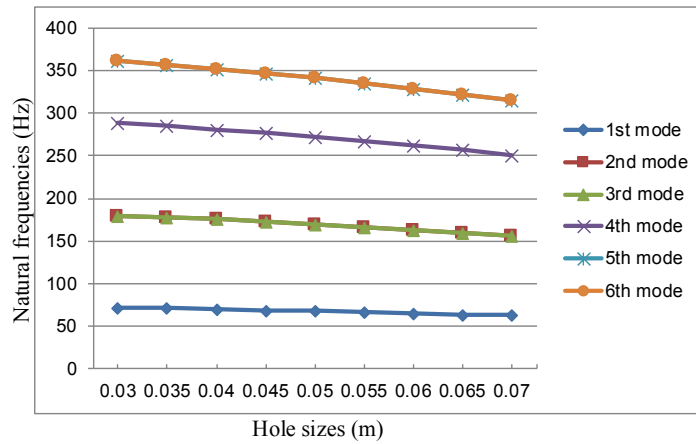
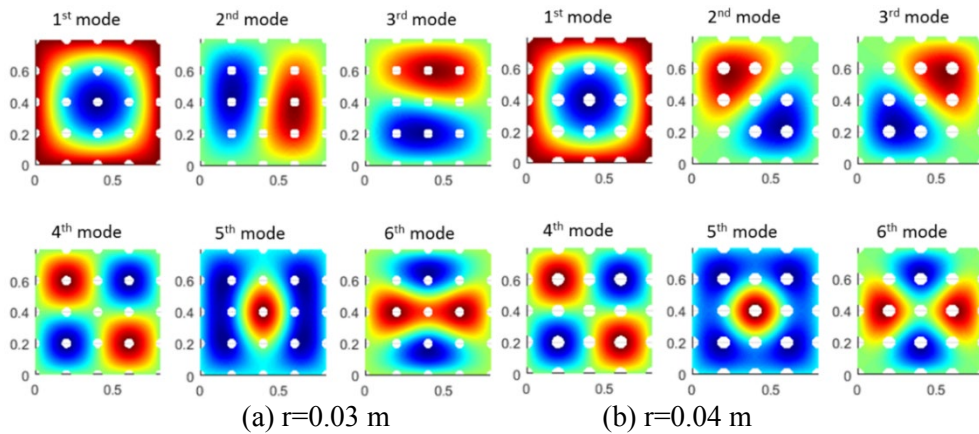


Figure 13: First six natural frequencies of the perforated plate (Hz)



(a) $r=0.03$ m

(b) $r=0.04$ m

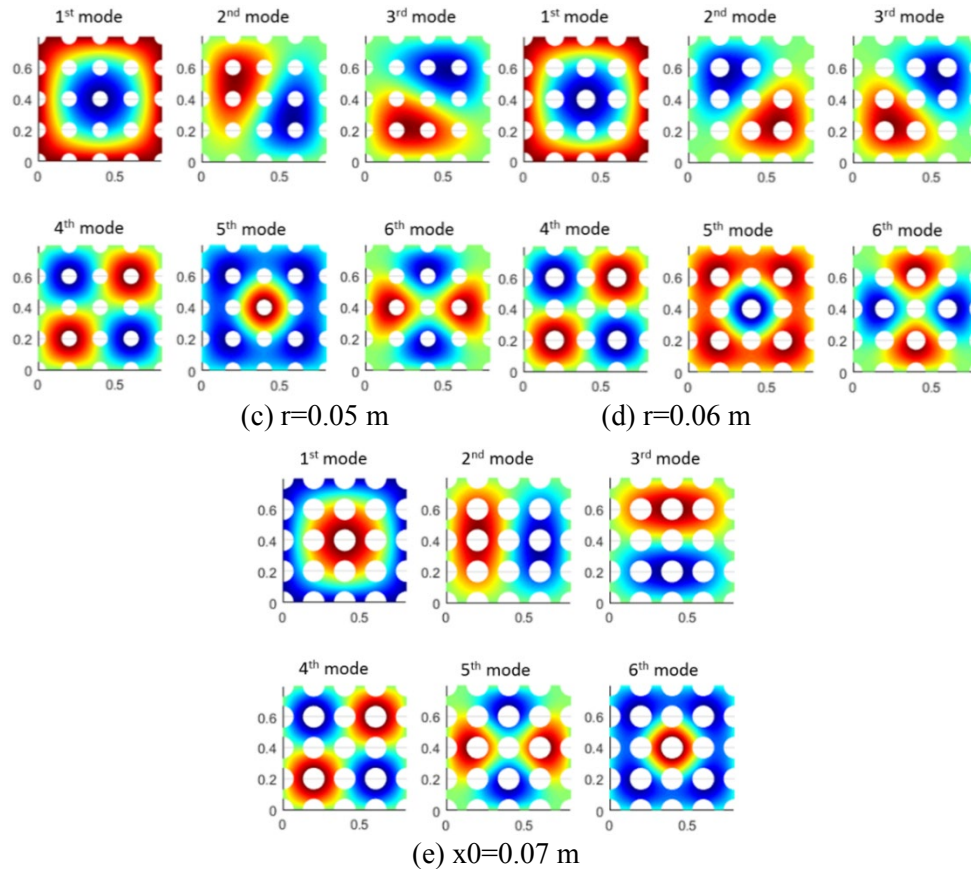


Figure 14: First six mode shapes of the perforated plate

4 Conclusions

A novel infinite element method is presented for solving Mindlin-Reissner plate vibration problems in this study. In the proposed method, the substructure domain is partitioned into multiple layers of geometrically similar finite elements, which use only the data of the boundary nodes, and the degree of freedom of the model is reduced using Craig-Bampton (CB) method. The convergence analysis of element layers involves only the mass matrix of the first element layer. Furthermore, in Craig-Bampton (CB) reduction process, the inversion of the symmetric block-tridiagonal global stiffness matrix has been determined only using the stiffness matrix of the first element layer. The validity of the proposed IEM has been demonstrated by means of four familiar examples involving a rectangular plate, a side cracked plate, a multiple point supported plate, and a perforated plate. The first example has demonstrated the general feasibility and accuracy of the proposed method. The second example considers a rectangular plate containing a through-thickness crack. The results show that the fourth and fifth frequencies are highly sensitive to the crack length. The third example considers a four point supported plate. The results show that the rectangular plate begins to weaken apparently when the support position x_0 is shifted over 0.25 m. The fourth example considers a perforated plate. The results show that the plate

starts to weaken but is not apparent when the hole becomes larger. The above examples show the advantages of IEM for singularity problems and geometric parametric analysis. In general, the results presented in this study have shown that the proposed method provides a direct, convenient and accurate tool for eigenvalue analysis of thin plate structure with complicated shapes.

Acknowledgement: This work was partially supported by the Advanced Institute of Manufacturing with High-tech Innovations (AIM-HI) from The Featured Areas Research Center Program within the framework of the Higher Education Sprout Project by the Ministry of Education (MOE) in Taiwan. This research was also supported by R.O.C. MOST Foundation Contract No. MOST108-3017-F-194 -001.

References

- Craig, J. R. R.; Bampton, M. C. C.** (1968): Coupling of substructures for dynamic analyses. *AIAA Journal*, vol. 6, pp. 1313-1319.
- Gupta, S.; Hussein, M. F. M.; Degrande, G.; Hunt, H. E. M.; Clouteau, D.** (2007): A comparison of two numerical models for the prediction of vibrations from underground railway traffic. *Soil Dynamics and Earthquake Engineering*, vol. 27, no. 7, pp. 608-624.
- Guyan, R. J.** (1965): Reduction of stiffness and mass matrices. *AIAA Journal*, vol. 3, no. 2, pp. 380-380.
- Han, H. D.; Ying, L. A.** (1979): An iterative method in the finite element. *Mathematica Numerica Sinica*, vol. 1, pp. 91-99.
- Han, H. D.; Ying, L. A.** (1982): The infinite element method for eigenvalue problems. *Numerische Mathematik*, vol. 1, pp. 39-50.
- Hurty, W. C.** (1965): Dynamic analysis of structural systems using component modes. *AIAA Journal*, vol. 3, no. 4, pp. 678-685.
- Irons, B.** (1965): Structural eigenvalue problems-elimination of unwanted variables. *AIAA Journal*, vol. 3, no. 5, pp. 961-962.
- Jain, J.; Li, H.; Cauley, S.; Koh, C. K.; Balakrishnan, V.** (2007): Numerically stable algorithms for inversion of block tridiagonal and banded matrices. *Purdue ECE Technical Reports (Paper 357)*.
- Kidder, R. L.** (1973): Reduction of structural frequency equations. *AIAA Journal*, vol. 11, no. 6, pp. 892-892.
- Kim, B. S.; Kim, B. S.; Yoo, H. H.** (2010): Analysis of vibration characteristics of a full vehicle model using substructure synthesis method. *Transactions of the Korean Society of Mechanical Engineers A*, vol. 34, no. 5, pp. 519-525.
- Li, R.; Tian, Y.; Wang, P. C.; Shi, Y. F.; Wang, B.** (2016): New analytic free vibration solutions of rectangular thin plates resting on multiple point supports. *International Journal of Mechanical Sciences*, vol. 110, pp. 53-61.
- Liu, D. S.; Chiou, D. Y.** (2003a): A coupled IEM/FEM approach for solving the elastic problems with multiple cracks. *International Journal of Solids and Structures*, vol. 40, pp.

1973-1993.

Liu, D. S.; Chiou, D. Y. (2003b): 3D IEM formulation with an IEM/FEM coupling scheme for solving elastostatic problems. *Advances in Engineering Software*, vol. 34, pp. 309-320.

Liu, D. S.; Zhuang, Z. W.; Chung, C. L. (2009): Modeling of moisture diffusion in heterogeneous epoxy resin containing multiple randomly distributed particles using hybrid moisture element method. *Computers, Materials & Continua*, vol. 13, pp. 89-113.

Liu, D. S.; Tu, C. Y.; Chung, C. L. (2013): Coupled PIEM/FEM algorithm based on Mindlin-Reissner plate theory for bending analysis of plates with through-thickness hole. *Computer Modeling in Engineering & Sciences*, vol. 92, pp. 573-594.

Liu, D. S.; Lin, Y. H. (2016): Vibration analysis of the multiple-hole membrane by using the coupled DIEM-FE scheme. *Journal of Mechanics*, vol. 32, pp. 163-173.

Liu, D. S.; Chen, Y. W. (2018): Application of Craig-Bampton reduction technique and 2D dynamic infinite element modeling approach to membrane vibration problems. *Journal of Mechanics*, pp. 1-13.

Love, A. E. H. (1888): On the small free vibrations and deformations of thin elastic shells. *Philosophical Transactions of the Royal Society of London*, vol. 179, pp. 125-137.

Mindlin, R. D. (1951): Influence of rotatory inertia and shear on flexural motions of isotropic, elastic plates. *ASME Journal of Applied Mechanics*, vol. 18, pp. 31-38.

Saito, A.; Castanier, M. P.; Pierre, C. (2006): Efficient nonlinear vibration analysis of the forced response of rotating cracked blades. *ASME 2006 International Mechanical Engineering Congress and Exposition*, pp. 469-478.

Thatcher, R. W. (1975): Singularities in the solution of Laplace's equation in two dimensions. *Journal of the Institute of Mathematics and Its Applications*, vol. 16, pp. 303-319.

Ying, L. A. (1978): The infinite similar element method for calculating stress intensity factors. *Scientia Sinica*, vol. 21, pp. 19-43.

Ying, L. A. (1992): An introduction to the infinite element method. *Mathematics in Practice Theory*, vol. 2, pp. 69-78.